

Accepted Manuscript

Title: Graphene oxide-deposited tilted fiber grating for ultrafast humidity sensing and human breath monitoring

Authors: Biqiang Jiang, Zhixuan Bi, Zhen Hao, Qingchen Yuan, Dingyi Feng, Kaiming Zhou, Lin Zhang, Xuetao Gan, Jianlin Zhao



PII: S0925-4005(19)30718-X
DOI: <https://doi.org/10.1016/j.snb.2019.05.024>
Reference: SNB 26547

To appear in: *Sensors and Actuators B*

Received date: 3 February 2019
Revised date: 22 April 2019
Accepted date: 8 May 2019

Please cite this article as: Jiang B, Bi Z, Hao Z, Yuan Q, Feng D, Zhou K, Zhang L, Gan X, Zhao J, Graphene oxide-deposited tilted fiber grating for ultrafast humidity sensing and human breath monitoring, *Sensors and amp; Actuators: B. Chemical* (2019), <https://doi.org/10.1016/j.snb.2019.05.024>

This is a PDF file of an unedited manuscript that has been accepted for publication. As a service to our customers we are providing this early version of the manuscript. The manuscript will undergo copyediting, typesetting, and review of the resulting proof before it is published in its final form. Please note that during the production process errors may be discovered which could affect the content, and all legal disclaimers that apply to the journal pertain.

Graphene oxide-deposited tilted fiber grating for ultrafast humidity sensing and human breath monitoring

Biqiang Jiang ^a, Zhixuan Bi ^a, Zhen Hao ^a, Qingchen Yuan ^a, Dingyi Feng ^a, Kaiming Zhou ^b, Lin Zhang ^b, Xuetao Gan ^{a,*}, and Jianlin Zhao ^{a,*}

^aMOE Key Laboratory of Material Physics and Chemistry Under Extraordinary Conditions and Shaanxi Key Laboratory of Optical Information Technology, School of Science, Northwestern Polytechnical University, Xi'an 710072, China

^bAston Institute of Photonic Technologies, Aston University, Birmingham B4 7ET, United Kingdom

*Corresponding authors. Email addresses: xuetaogan@nwpu.edu.cn (X. Gan); jlzhao@nwpu.edu.cn (J. Zhao)

Highlights

1. An optical fiber-based humidity sensor with ultrafast response is proposed by depositing GO onto a tilted fiber grating (TFG) with large tilted angle.
2. The experimental results show sensitivities of 18.5 pm/%RH and 0.02 dB/%RH with highly linear coefficient in the dynamic range of 30%-80%RH.
3. The sensor is successfully applied to monitor human breathing cycles with different breathing frequencies.
4. The sensor also shows the properties of easy fabrication, low hysteresis, ultrafast response, and high repeatability and reliability.

Abstract: We propose and experimentally demonstrate a high-performance relative humidity (RH) sensor by depositing graphene oxide (GO) onto tilted fiber grating (TFG). The largely tilted grating planes of the employed TFG can induce a set of polarization-dependent cladding modes and strong evanescent field to couple with the humidity-dependent dielectric of GO layer. The GO-deposited TFG presents the response sensitivities of 18.5 pm/%RH and 0.027 dB/%RH in the range of 30%~80%RH by tracking the wavelength and intensity of a specific cladding mode resonance. By monitoring the human breath with different frequencies, the sensor exhibits an ultrafast response within ~42 ms due to the thin GO film and unimpeded permeation of water molecules through GO interlayer. The easy fabrication, low hysteresis, fast response, and high repeatability and reliability of the proposed RH sensor may enable many potential applications including pharmaceutical processing, human health and environmental monitoring.

Keywords: Humidity sensor, graphene oxide, tilted fiber grating, human breath monitoring.

1. Introduction

Humidity is an essential index of environmental monitoring, and the measurement of humidity has been extensively used in food processing, electronic products, pharmaceutical manufacturing, precision instrument laboratories, and even the control of human comfort and health [1, 2]. Among a variety of humidity sensors, the use of fiber-optic devices presents unique advantages of compact size, light weight, low cost, immune to electromagnetic interference, and remote and distributed measurement. Many fiber-based schemes have been developed for humidity sensing, including etched/tapered/polished fibers [3-6], hollow core fibers [7], and grating-assisted fibers including fiber Bragg gratings (FBGs) [8-12], tilted FBGs (TFBGs) [13-15] and long-period gratings (LPGs) [16, 17]. Actually, determined by fiber's silica-based material properties, these fiber devices such as FBGs are intrinsically sensitive to only physical parameters (i.e. temperature and strain). For the purpose of humidity sensing, hygroscopic materials are always required to be coated onto the surface of fiber devices. For example, FBGs only with core mode have to be coated with thick materials with hygroscopic expansion effect to sense the change of humidity [9, 18]. On the other hand, by integrating materials with moisture-sensitive refractive index onto fiber devices with evanescent fields or cladding modes, humidity sensing could be carried out. Normally, polymers (polyimide, polyvinyl alcohol, etc.) with moisture absorption are chosen to coat on tapered, etched, polished, hollow-core fibers and TFBG to fabricate the humidity sensors [3-7, 13]. Unfortunately, these polymer-based hygroscopic materials have a relatively slow humidity response and considerable hysteresis.

Recently, graphene oxide (GO), the most important derivatives of graphene, is considered as a very promising material for humidity sensing. Different from the porous material structures of polymers, GO has high surface-area-to-volume ratio and strong absorption property in a wide wavelength range, and can be integrated with optical fiber for UVA and biochemical sensing [19-21]. More importantly, there are rich oxygen-coating groups between layers for interacting with water molecules, such as hydrophilic hydroxyl, epoxy, and carboxylic groups [1]. In addition, these groups provide a channel for superpermeability to water molecules, which could facilitate their fast interaction processes between water molecules and GO layers, and thus can be developed in humidity sensing devices [14, 22-26].

In this work, we deposit GO film onto a tilted fiber grating (TFG) to implement a high-performance relative humidity (RH) sensor relying on GO's unique attributes. Compared with the TFBG, the employed TFG has so large tilted angle breaking the fiber's azimuthal symmetry, and thus could excite a set of polarization-dependent cladding modes and induce the strong evanescent field [27, 28]. It is also called "excessively tilted" fiber grating. Therefore, the lightwave propagation in such TFG could be effectively modified by the coated GO via its interaction with cladding modes, enabling a sensitive humidity measurement. In the fabrication of fiber devices, the TFG transmission shows a highly sensitive evolution as the GO disposition thickness. By tracking

the resonant wavelength and intensity of a specific cladding mode, the GO-deposited TFG exhibits the response sensitivities of 18.5 pm/%RH and 0.027 dB/%RH with good linearity and low hysteresis in the range of 30%~80%RH. The sensor is also applied in real-time monitoring the human breathing with different frequencies, showing an ultrafast and reversible response of ~42 ms response time. Different from geometry-modified fibers which require complicated processes of etching, polishing, or tapering, the TFGs retaining a robust mechanical structure have been used for light-matter interaction and bio/chemical sensing [29-32]. The reliabilities of easy fabrication and GO integration, combining with the high sensing performances, promise many potential applications in pharmaceutical processing, human health and environmental monitoring.

2. Tilted fiber grating with large tilted angle

The TFG is a special member in the fiber grating family whose grating planes are angled by a certain degree with respect to the fiber axis, as schematically shown in Fig. 1(a). In this work, the employed TFG has a tilted angle of more than 80 degree. The grating period along the fiber axis is much larger than that of the initial period determined by the phase mask, and thus the forward-propagating core mode will be coupled into forward-propagating cladding modes [33]. The largely tilted fringes will locally break the cylindrical symmetry of the fiber core and induce a strong birefringent effect, and then the TFG demonstrates a noticeable multi-notch dual-peak feature [32], including two orthogonal resonance peaks of transverse electric and transverse magnetic cladding modes. Determined by the phase matching condition, the resonant wavelength of the m th cladding mode can be expressed as follows:

$$\lambda_{i,\text{clad}}^m = \left[n_{\text{eff,core}} - n_{i,\text{eff,clad}}^m \right] \Lambda_g / \cos \theta, \quad (1)$$

where, i represents the two orthogonal mode resonances, Λ_g is the period perpendicular to the grating planes, θ is the tilted angle, and $n_{\text{eff,core}}$ and $n_{i,\text{eff,clad}}^m$ represent the effective indices of the core mode and the m th cladding mode, respectively. Also from Eq. (1), the surrounding medium's refractive index can affect the effective index of the cladding modes and then the resonant wavelengths, which shows the fundamental principle for environmental parameters sensing.

In the experiment, we fabricated the TFG in hydrogenated (for photosensitivity enhancement of fiber core) single mode fiber by using the scanning phase-mask technique and a frequency doubled continuous wave Ar⁺ laser (wavelength of 244nm). The UV laser beam was focused on the fiber core by a cylindrical lens, and the phase mask with a period of 6.6 μm was slanted with respect to the fiber axis, with the angle as a key factor to determine the excitation of the cladding modes and sensing capacity to the surroundings. After UV inscription, the TFG was annealed at 80°C for 48 hours to stabilize and remove residual hydrogen. Figure 1(b) shows the optical microscope image of the tilted fringes in the fiber core of the TFG examined by a high-resolution microscope. The tilted angle of the grating plane is ~82°, and the grating length is 15mm. The transverse field distribution of the core mode and high-order cladding mode are simulated by using the finite element

method, and the results are shown in Figure 1(c). Clearly, the light field can be extended into the cladding and even to the fiber boundary, which promises the interaction with the surroundings or coating layer.

3. Surface modification and characterization

To enhance the RH sensitivity of TFG, it is necessary to modify the fiber surface by depositing the GO layer with abundant hydrophilic groups. A GO aqueous suspension with the concentration of 2 mg/ml and the average nanosheet size of 50-200nm was purchased from Nanjing XFNANO Materials Tech Co., Ltd, China. The employed TFG was firstly soaked in HNO_3 solution (5% v/v) for 1 hour at room temperature to remove the contaminant, and then thoroughly rinsed with deionized (DI) water and ethanol for several times. The GO suspension was deposited on the surface of the TFG by using a dip-coating technique [34]. For uniform GO deposition, two ends of the TFG were clamped with two stages to keep the fiber straight and stationary. A multiple deposition method was used to achieve the required sensitivity and precisely control the thickness of the GO deposition. After each new monolayer is deposited onto it for taking preliminary RH measurements. For each time, the grating region was immersed in the GO suspension for 20 min, and then naturally dried in air for 5 min.

During the depositing process, the transmission spectrum of the TFG was monitored and recorded in real-time with an optical spectrum analyzer (OSA). Figure 2 shows the spectral evolution with the deposition times. As the deposition time increases, the spectrum gradually shifts and attenuates as a result of the interaction between the cladding modes and the thicker GO layer with a complex refractive index. The resonant wavelength red-shifts by ~ 3 nm due to the high refractive index of GO layer. Therefore, the deposition of GO onto the TFG can be initially evaluated according to the spectrum change of TFG.

After each GO deposition, the TFG was placed over a drop of water for the tentative RH measurement. Since the environmental RH of the lab is $\sim 55\%$, and the RH will be up to $>80\%$ over the water drop, we could record and compare both spectra of the two cases. The results after the 28th deposition are shown in Fig. 3(a). A significant wavelength shift was induced by the RH change when the TFG was placed at a distance of about 1mm above the water drop. When the spectrum-shift reached a maximum value, we stopped this deposition process. It is therefore possible to find an optimal deposition thickness. Figure 3(b) gives the detailed results, showing the RH responses as a function of deposition time. The spectrum shift reached the maximum value of ~ 0.5 nm after the deposition time of ~ 450 min.

The employed multiple deposition method will result in a relatively uniform GO layer and allow a controllable thickness. After the deposition, an optical microscope with high resolution was used to characterize the surface morphology of the GO-deposited TFG. Figures 4(a) and 4(b) display the microscope images before and after GO deposition, showing the GO film tightly and smoothly deposited around the TFG surface. The zoomed cross-section of GO-deposited TFG was also

examined by scanning electron microscopy (SEM), as shown in Fig. 4(c). The thickness of GO deposition is ~54 nm. Due to the unique Raman scattering properties of GO, we further characterized the TFG surface without and with GO deposition layer by a Raman system at 432nm laser excitation. Figure 4(d) plots the measured Raman spectra. Compared with the spectrum of the bare one, the prominent bands can be observed around 1348 cm^{-1} and 1598 cm^{-1} , which verifies the D and G Raman vibrational modes of graphitic carbon sheet, respectively [35]. The G band reflects the first-order scattering of the in-plane optical phonon E_{2g} mode, and D band is induced by the boundary effect of the presence of structural imperfections and the attachment of hydroxyl and epoxide groups [34, 36]. The above characterizations revealed that the GO was effectively and tightly modified on the TFG surface.

4. Experiment results and discussions

To examine the RH response, the fabricated sensor was fixed and sealed in a home-made gas chamber, and a commercial hygrometer with the accuracy of 0.1%RH was embedded inside to measure the real-time RH. Figure 5 schematically depicts the experimental setup for examining the RH sensing performance. Light from a broadband supercontinuum (superK) source was launched into the GO-deposited TFG via a fiber polarizer and polarization controller (PC) to adjust the polarization state of input light, and the transmission spectra were monitored by the OSA. For the RH control module, the dry nitrogen from the gas cylinder was divided two paths with a Y-tube, and each path connected a flowmeter to control the flow rate. One of the paths was inserted into the pure water to generate the saturated humid gas. Then, the two paths were mixed with another Y-tube to the inlet of the chamber, thus the RH level inside could be controlled by individually adjustable flow rates [24, 37].

The maximum range of RH level controlled by our gas humidity module is 25%~85%. In the measurement, we increased the RH from 30% to 80% and then gradually decrease to the initial state. To avoid the temperature effect on the RH test, we kept track of the room temperature variation during the experiment. Figure 6(a) shows the spectra of the GO-deposited TFG with different RH levels at a given room temperature (~22°C), monitoring two resonance modes in the range of 1490~1570nm. Clearly, as the RH increasing, the GO film around the TFG absorbed more water vapors and induced an increase of the refractive index, resulting in a redshift of the resonant wavelengths and an attenuation of coupling intensity. The results are plotted in Fig. 6(b). In the range of 30%~80%RH, the extracted resonant wavelength and coupling intensity linearly change with the increasing RH, and the corresponding response coefficients from the linear fitting results are 18.5 pm/%RH with the *R*-square value of 0.998 and 0.027 dB/%RH with the *R*-square value of 0.994, respectively. The RH sensitivity is much higher than that of bare TFG which almost remains unchanged with RH variation. The RH response of Dip 2 has a similar measurement result.

The sensing enhancement of TFG with GO deposition can be explained by the permeation mechanism of water molecules into the GO layer. It has been proved that GO membranes which are

a collection of micro-sized crystallites stacked on each other, have high performance for the detection of vapor molecules [38]. The hydroxyl and epoxide groups attached to graphene sheets are helpful in keeping the relative large interlayer distance of the crystallites, and form the two-dimensional GO nanochannels allowing low-friction flow of monolayer water. The transport speed of water molecules in the channels formed by the gaps between micro-sized crystallites is close to $1 \text{ m}\cdot\text{s}^{-1}$ [39], which is responsible for the fast response properties of GO-based humidity sensors, and also can be verified by the next experiment. Differential pressure occurs as the increase of humidity, leading to the growth of the interlayer distance, and then more water molecules fill into the GO capillaries, leading to the increase of the refractive index of GO laminates and the shift of the TFG resonance wavelength. More importantly, the process of absorption and desorption of moisture was found to be reversible with varying RH [38].

The hysteresis response of the fabricated sensor was measured by ascending and descending RH level from 30% to 80%. Figure 6(c) shows the results of the two measurements. The sensor shows very low hysteresis and stable RH response. Especially in the low RH level, there is almost no changes in the spectrum, as shown in the inset of Fig. 6(c). The GO-deposited TFG can therefore be reversible due to the absorption and desorption of GO to water molecules.

As aforementioned, the larger interlayer spacing for low-friction flow of monolayer water due to abundant hydroxyl and epoxide groups of GO will be expected to achieve the RH sensing with a fast response. To obtain the response time, we directly monitored a human breath with different breathing frequencies. The resonant dip of the GO-deposited TFG was considered as an edge filter, and a narrowband light signal with the bandwidth of $\sim 0.2 \text{ nm}$ from a tunable laser was launched into the TFG. The narrowband light was fixed at the wavelength close to the resonant dip, and then the output light power was detected with a photodetector and displayed with an oscilloscope. Since the human breathing contains much water vapors, the wavelength shift of the resonant dip will lead to the power decrease of transmission. Figure 7 shows the periodical change of transmission power with the rhythmically breathing wet-air interacting with the GO-deposited TFG. The transmission power or the converted voltage immediately rise with both normal (test 1) and rapid breathing (test 2), as shown in the top and bottom parts of Fig. 7(a), respectively. According to Fast Fourier Transformation (FFT) results shown in Fig. 7(b), the breathing frequencies of the two tests are 0.7 Hz and 1.1 Hz, respectively. As revealed in Fig. 7(c), the response and recovery times are calculated as $\sim 42 \text{ ms}$ and $\sim 115 \text{ ms}$, respectively. The recovery time in the desorption process of moisture is longer than the response time in the absorption process of moisture. In addition, the periodically reversible maximum and minimum powers and the aforementioned low hysteresis reveal that the proposed sensor has a good repeatability and reliability during the breathing cycles.

From Table 1, the sensitivity of the proposed sensor is roughly equivalent to other fiber-based RH sensors. However, owing to GO's superpermeability to water molecules and only 54nm-thick layer, the fabricated RH sensor exhibits the fastest response speed. For instance, PVA, PMMA or polyimide based (or coated) FBG/TFBG have the response time of more than 2 s even to 22 min[8,

9, 13, 18], Di-ureasil coated FBG has the response time of 8.1 min [10]. It should be noted that there are also some (reduced) GO-coated hollow core fiber, polished fiber or TFBG for humidity sensing, however they show the longer response time of 1~5.2 s limited by the thicker GO layer with submicron-to-micron thickness [5, 7, 14]. Therefore, this fast response and recovery time of the fabricated sensor can achieve the human breath monitoring in real-time. Moreover, different from stain- or temperature-based breath monitoring techniques [40, 41], the proposed scheme is non-contact monitoring and can detect the breath depth distinguished by the amplitude of the output waveforms.

Table 1. Comparison of sensing performance between optical fiber-based RH sensors.

Sensor	Range (RH)	Sensitivity	Response	Recovery
Polished fiber with rGO [5]	75%-95%	0.31 dB/%RH	5 s	15 s
rGO-coated hollow core fiber [7]	60%-90%	0.22 dB/%RH	5.2 s	8.1 s
GO-coated TFBG [14]	10%~80%	0.129 dB/%RH	1 s	NA
GO-coated etched-TFBG [15]	20%~80%	0.01 nm/%RH	12.25 min	21.75 min
PVA coated hybrid fiber grating [8]	30%-95%	Nonlinear, ~0.737 nW/%RH	~2 s	NA
Polyimide coated FBG [9]	20%-90%	0.00171 nm/%RH	>33 s	NA
Di-ureasil coated FBG [10]	15%-95%	0.022 nm/%RH	8.1 min	NA
Polymer FBG [11]	50%-95%	0.035 nm/%RH	30 min	NA
TFBG with PVA [13]	20%-98%	2.52 dBm/%RH	2 s	NA
Polyimide coated FBG [18]	12%-97%	0.0136 nm/%RH	22 min	NA
GO-deposited TFG (This work)	> (30%-80%)	0.0185 nm/%RH	0.042 s	0.115 s

5. Conclusions

In summary, an optical fiber-based humidity sensor with ultrafast response is proposed and experimentally demonstrated. By depositing GO onto the surface of TFG with large tilted angle, the structure supports strong interactions between the cladding mode resonances and GO layer. The intensity and wavelength of cladding mode resonances of the TFG vary with the GO depositing due to the complex refractive index property. The investigations of optical microscopy, SEM, Raman spectroscopy verify effective and tight GO deposition. Since the absorption of moisture changes the effective index of cladding modes, the transmission spectrum of the TFG shows a linear spectrum redshift and power responses with the increase of RH level. The experimental results show sensitivities of 18.5 pm/%RH and 0.02 dB/%RH with highly linear coefficient in the dynamic range of 30%-80%RH. In addition, the sensor is successfully applied to monitor human breathing cycles with different frequencies, which exhibits a response time within tens of milliseconds due to the thin GO layer. Therefore, the proposed all-in-fiber RH sensor with high reversibility, repeatability, and especially ultrafast response is a promising alternative for situations where the device compactness and dynamic RH change are required, such as industrial process controls, meteorology, and various medical diagnostics including human breath monitoring.

Acknowledgement

This work was supported by the National Natural Science Foundation of China (Grants No. 61775182, 61505165, and 61522507). We also would like to thank the Analytical & Testing Center of Northwestern Polytechnical University for SEM test.

References

- [1] H. Chi, Y.J. Liu, F. Wang, C. He, Highly Sensitive and Fast Response Colorimetric Humidity Sensors Based on Graphene Oxides Film, *ACS Appl. Mater. Inter.*, 7(2015) 19882-19886.
- [2] D.L. Presti, C. Massaroni, E. Schena, Optical Fiber Gratings for Humidity Measurements: A Review, *IEEE Sensors Journal*, 18(2018) 9065-9074.
- [3] Y. Luo, C. Chen, K. Xia, S. Peng, H. Guan, J. Tang, et al., Tungsten disulfide (WS₂) based all-fiber-optic humidity sensor, *Opt. Express*, 24(2016) 8956-8966.
- [4] B. Du, D. Yang, X. She, Y. Yuan, D. Mao, Y. Jiang, et al., MoS₂-based all-fiber humidity sensor for monitoring human breath with fast response and recovery, *Sens. Actuators B Chem.*, 251(2017) 180-184.
- [5] Y. Xiao, J. Zhang, X. Cai, S. Tan, J. Yu, H. Lu, et al., Reduced graphene oxide for fiber-optic humidity sensing, *Opt. Express*, 22(2014) 31555-31567.
- [6] J.M. Corres, J. Bravo, I.R. Matias, F.J. Arregui, Nonadiabatic tapered single-mode fiber coated with humidity sensitive nanofilms, *IEEE Photon. Technol. Lett.*, 18(2006) 935-937.
- [7] R. Gao, D.-f. Lu, J. Cheng, Y. Jiang, L. Jiang, Z.-m. Qi, Humidity sensor based on power leakage at resonance wavelengths of a hollow core fiber coated with reduced graphene oxide, *Sens. Actuators B Chem.*, 222(2016) 618-624.
- [8] X.Y. Dong, T. Li, Y. Liu, Y. Li, C.L. Zhao, C.C. Chan, Polyvinyl alcohol-coated hybrid fiber grating for relative humidity sensing, *J. Biomed. Opt.*, 16(2011) 4.
- [9] W. Wang, T. Sun, J. Peng, J. Dai, M. Yang, Humidity sensor based on fiber Bragg grating coated with different pore-foaming agent doped polyimides, *IEEE Photon. Technol. Lett.*, 29(2017) 1963-1966.
- [10] S.F.H. Correia, P. Antunes, E. Pecoraro, P.P. Lima, H. Varum, L.D. Carlos, et al., Optical fiber relative humidity sensor based on a FBG with a Di-ureasil coating, *Sensors*, 12(2012) 8847-8860.
- [11] C. Zhang, W. Zhang, D.J. Webb, G. Peng, Optical fibre temperature and humidity sensor, *Electron. Lett.*, 46(2010) 643-644.
- [12] W. Zhang, D.J. Webb, G. Peng, Investigation Into Time Response of Polymer Fiber Bragg Grating Based Humidity Sensors, *J. Lightwave Technol.*, 30(2012) 1090-1096.
- [13] Y. Miao, B. Liu, H. Zhang, Y. Li, H. Zhou, H. Sun, et al., Relative humidity sensor based on tilted fiber Bragg grating with polyvinyl alcohol coating, *IEEE Photon. Technol. Lett.*, 21(2009) 441-443.
- [14] Y. Wang, C. Shen, W. Lou, F. Shentu, C. Zhong, X. Dong, et al., Fiber optic relative humidity sensor based on the tilted fiber Bragg grating coated with graphene oxide, *Appl. Phys. Lett.*, 109(2016) 031107.
- [15] Y.-D. Chiu, C.-W. Wu, C.-C. Chiang, Tilted fiber Bragg grating sensor with graphene oxide coating for humidity sensing, *Sensors*, 17(2017) 2129.
- [16] M. Consales, G. Berruti, A. Borriello, M. Giordano, S. Buontempo, G. Breglio, et al., Nanoscale TiO₂-coated LPGs as radiation-tolerant humidity sensors for high-energy physics applications,

- Opt. Lett., 39(2014) 4128-4131.
- [17] X. Yu, P. Childs, M. Zhang, Y. Liao, J. Ju, W. Jin, Relative humidity sensor based on cascaded long-period gratings with hydrogel coatings and Fourier demodulation, IEEE Photon. Technol. Lett., 21(2009) 1828-1830.
- [18] Y. Lin, Y. Gong, Y. Wu, H.J. Wu, Polyimide-Coated Fiber Bragg Grating for Relative Humidity Sensing, Photonic Sensors, 5(2015) 60-66.
- [19] P. Lesiak, S. Ł., M. Bieda, P. Sobotka, A. Dużyńska, A. Wróblewska, et al., UVA sensor based on highly birefringent fiber covered with graphene oxide, IEEE Photon. Technol. Lett., 30(2018) 845-848.
- [20] A.A. Shabaneh, S.H. Girei, P.T. Arasu, W.B.W.A. Rahman, A.A.A. Bakar, A.Z. Sadek, et al., Reflectance response of tapered optical fiber coated with graphene oxide nanostructured thin film for aqueous ethanol sensing, Opt. Commun., 331(2014) 320-324.
- [21] Sridevi S, K.S. Vasu, N. Jayaraman, S. Asokan, A.K. Sood, Optical bio-sensing devices based on etched fiber Bragg gratings coated with carbon nanotubes and graphene oxide along with a specific dendrimer, Sens. Actuators B Chem., 195(2014) 150-155.
- [22] K.-L. Zhang, Z.-L. Hou, B.-X. Zhang, Q.-L. Zhao, Highly sensitive humidity sensor based on graphene oxide foam, Appl. Phys. Lett., 111(2017) 153101.
- [23] Z. Wang, Y. Xiao, X. Cui, P. Cheng, B. Wang, Y. Gao, et al., Humidity-Sensing Properties of Urchinlike CuO Nanostructures Modified by Reduced Graphene Oxide, ACS Appl. Mater. Inter., 6(2014) 3888-3895.
- [24] X. Gan, C. Zhao, Q. Yuan, L. Fang, Y. Li, J. Yin, et al., High performance graphene oxide-based humidity sensor integrated on a photonic crystal cavity, Appl. Phys. Lett., 110(2017) 151107.
- [25] S. Borini, R. White, D. Wei, M. Astley, S. Haque, E. Spigone, et al., Ultrafast Graphene Oxide Humidity Sensors, ACS Nano, 7(2013) 11166-11173.
- [26] W. Xuan, X. He, J. Chen, W. Wang, X. Wang, Y. Xu, et al., High sensitivity flexible Lamb-wave humidity sensors with a graphene oxide sensing layer, Nanoscale, 7(2015) 7430-7436.
- [27] Z. Yan, H. Wang, C. Wang, Z. Sun, G. Yin, K. Zhou, et al., Theoretical and experimental analysis of excessively tilted fiber gratings, Opt. Express, 24(2016) 12107-12115.
- [28] K. Zhou, L. Zhang, X. Chen, I. Bennion, Optic sensors of high refractive-index responsivity and low thermal cross sensitivity that use fiber Bragg gratings of $>80^\circ$ tilted structures, Opt. Lett., 31(2006) 1193-1195.
- [29] B. Luo, Z. Yan, Z. Sun, J. Li, L. Zhang, Novel glucose sensor based on enzyme-immobilized 81° tilted fiber grating, Opt. Express, 22(2014) 30571-30578.
- [30] B. Jiang, K. Zhou, C. Wang, Q. Sun, G. Yin, Z. Tai, et al., Label-free glucose biosensor based on enzymatic graphene oxide-functionalized tilted fiber grating, Sens. Actuators B Chem., 254(2018) 1033-1039.
- [31] Z. Yan, Z. Sun, K. Zhou, B. Luo, J. Li, H. Wang, et al., Numerical and experimental analysis of sensitivity-enhanced RI sensor based on Ex-TFG in thin cladding fiber, J. Lightwave Technol., 33(2015) 3023-3027.
- [32] B. Jiang, G. Yin, K. Zhou, C. Wang, X. Gan, J. Zhao, et al., Graphene-induced unique polarization tuning properties of excessively tilted fiber grating, Opt. Lett., 41(2016) 5450-5453.
- [33] K. Zhou, L. Zhang, X. Chen, I. Bennion, Low thermal sensitivity grating devices based on Ex- 45° tilting structure capable of forward-propagating cladding modes coupling, J. Lightwave Technol., 24(2006) 5087-5094.

- [34] S.S. Gao, H.W. Qiu, C. Zhang, S.Z. Jiang, Z. Li, X.Y. Liu, et al., Absorbance response of a graphene oxide coated U-bent optical fiber sensor for aqueous ethanol detection, *RSC Adv.*, 6(2016) 15808-15815.
- [35] K.N. Kudin, B. Ozbas, H.C. Schniepp, R.K. Prud'homme, I.A. Aksay, R. Car, Raman spectra of graphite oxide and functionalized graphene sheets, *Nano Lett.*, 8(2008) 36-41.
- [36] A.C. Ferrari, J.C. Meyer, V. Scardaci, C. Casiraghi, M. Lazzeri, F. Mauri, et al., Raman Spectrum of Graphene and Graphene Layers, *Phys. Rev. Lett.*, 97(2006) 187401.
- [37] C. Zhao, Q. Yuan, L. Fang, X. Gan, J. Zhao, High-performance humidity sensor based on a polyvinyl alcohol-coated photonic crystal cavity, *Opt. Lett.*, 41(2016) 5515-5518.
- [38] R.R. Nair, H.A. Wu, P.N. Jayaram, I.V. Grigorieva, A.K. Geim, Unimpeded Permeation of Water Through Helium-Leak-Tight Graphene-Based Membranes, *Science*, 335(2012) 442-444.
- [39] B. Radha, A. Esfandiar, F.C. Wang, A.P. Rooney, K. Gopinadhan, A. Keerthi, et al., Molecular transport through capillaries made with atomic-scale precision, *Nature*, 538(2016) 222.
- [40] L. Dziuda, F.W. Skibniewski, M. Krej, P.M. Baran, Fiber Bragg grating-based sensor for monitoring respiration and heart activity during magnetic resonance imaging examinations, *J. Biomed. Opt.*, 18(2013) 057006.
- [41] A. Manujlo, T. Osuch, Temperature fiber Bragg grating based sensor for respiration monitoring: *Proc. SPIE*, 10445, 2017.

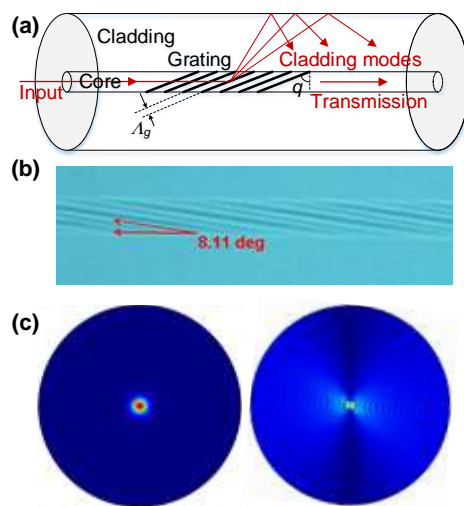


Fig. 1. (a) Schematic of the TFG with large tilted angle, (b) optical microscope image of the tilted fringes in the fiber core, and (c) simulated core mode and high-order cladding mode fields in the fiber.

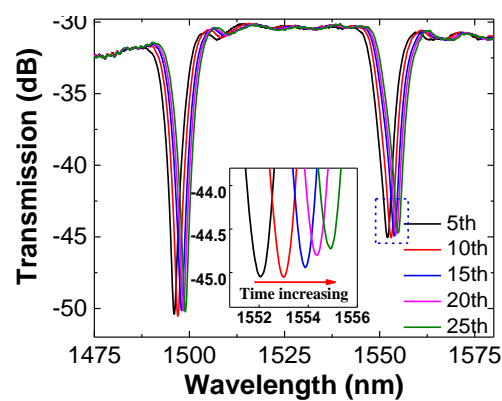


Fig. 2. Spectral evolution of the TFG during the GO depositions.

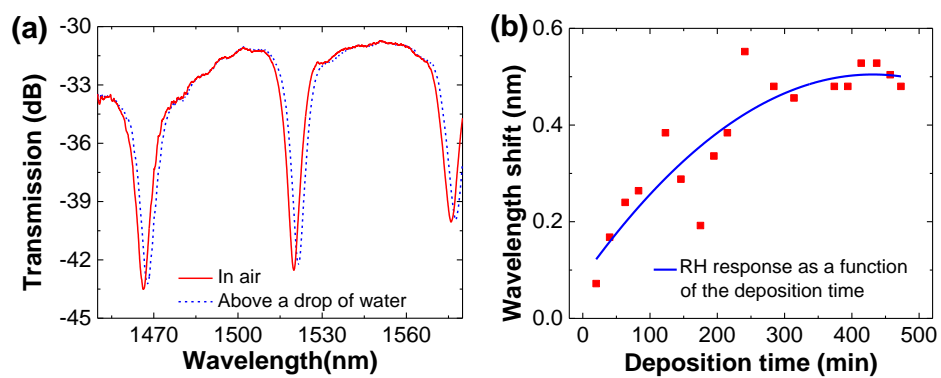


Fig. 3. (a) Spectrum shift of the TFG for a tentative RH test, and (b) the corresponding wavelength shift as a function of the deposition time.

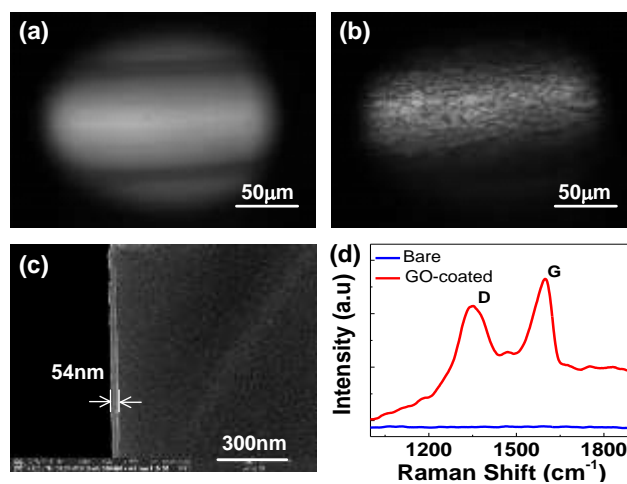


Fig. 4. Optical microscope images of (a) bare and GO-coated TFG at the magnification of 60×, (c) SEM image of the zoomed cross section of the GO-coated TFG, and (d) Raman spectra of bare and GO-coated TFG showing the G and D bands of GO.

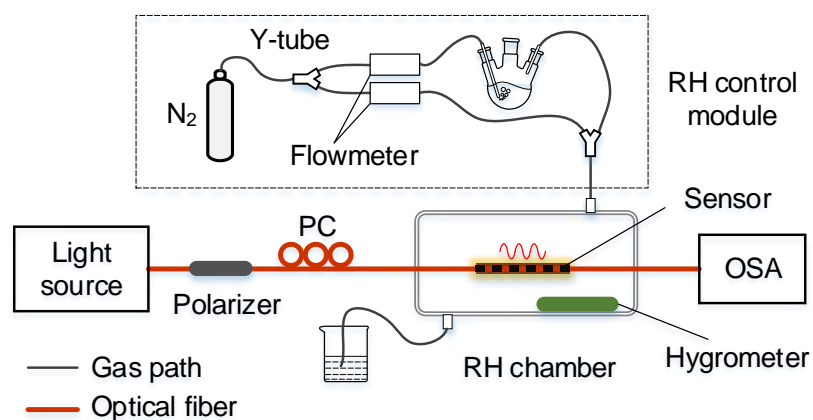


Fig. 5. Experimental setup of GO-deposited TFG for the RH response.

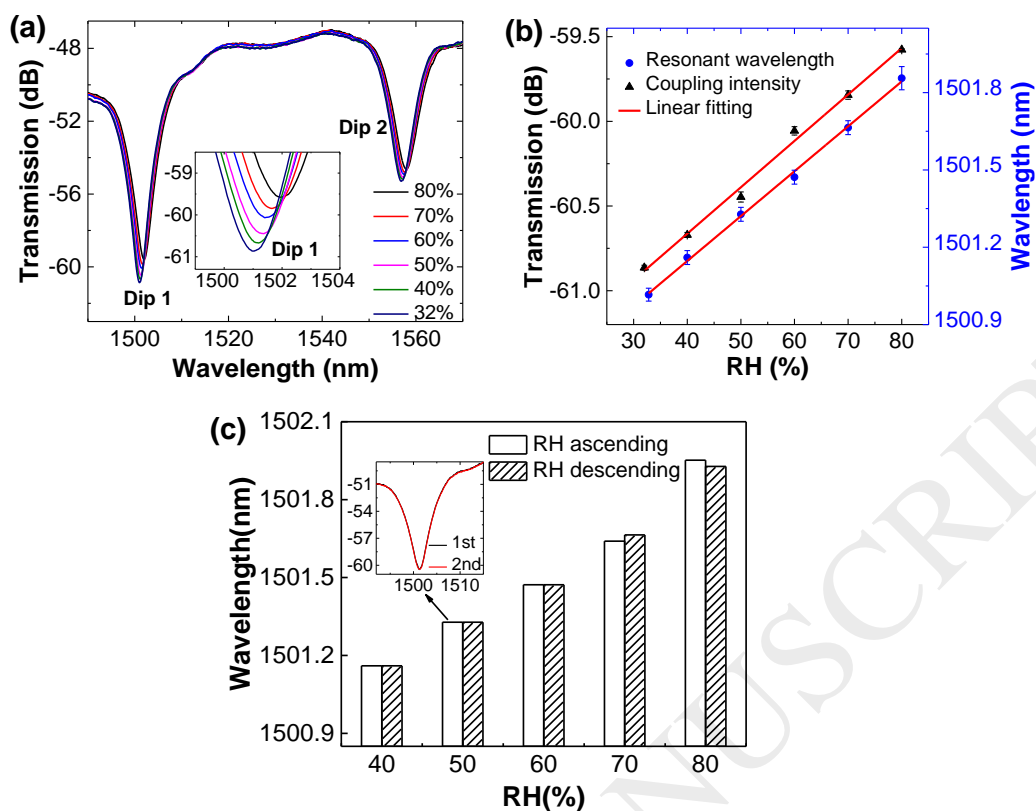


Fig. 6. (a) Spectral evolution of the GO-deposited TFG with varied RH levels; (b) Resonant wavelength and intensity of Dip 1 versus the RH level; (c) Hysteresis test of the RH response, and the inset is the spectra of GO-deposited TFG for repeated measurements at 50% RH.

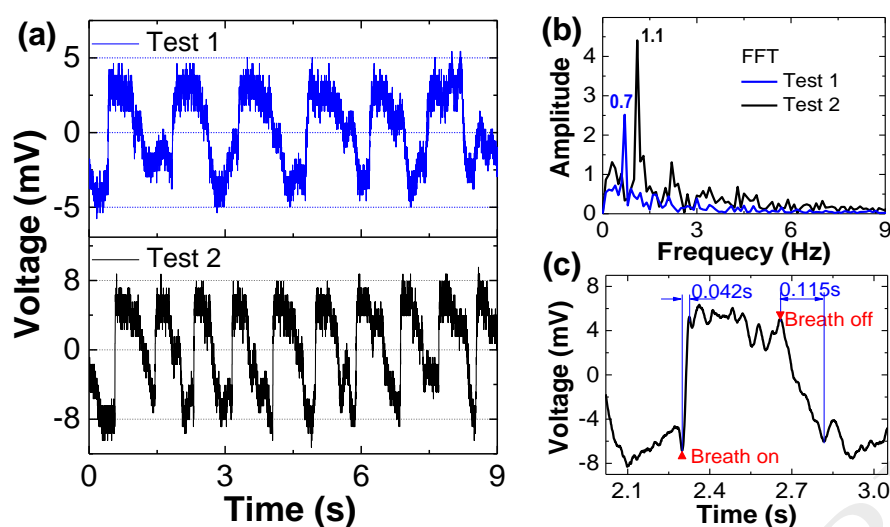


Fig. 7. (a) Responses of GO-deposited TFG to human breathing, including normal (top) and rapid (bottom) breathing, and (b) their FFT results, displaying different breathing frequencies. (c) Enlarged view of the temporal waveform to evaluate the response and recovery time.